

A fast defect detection algorithm for glass tube based on ROI reduction

Gabriele Antonio De Vitis, Pierfrancesco Foglia and Cosimo Antonio Prete
Dipartimento di Ingegneria dell'Informazione, Università di Pisa
Pisa, Italy

ABSTRACT

In this paper, we present an algorithm for defect detection in glass products that allows us to minimize the processing time. The main idea is based on the reduction of the size of the image area to investigate by using the features of glass images. Results on a set of test images show that the proposed solution does not compromise the quality of the detection and allows to achieve an improvement of a factor of 7x compared to the existing solution under particular conditions, with the same accuracy in defect detection

Keywords: Defect detection, glass production, real-time inspection, image processing, inspection systems.

1. INTRODUCTION

An inspection system for semi-finished glass production can be based on machine vision [1], [2], [3] and it is constituted by an Image Acquisition Subsystem and a Host Computer. The Image Acquisition Subsystem is devoted to the acquisition of the digitized images (frames); key components of such system are a LED-based illuminator, a line scan camera, and a frame grabber, which groups together single sequential lines captured by the camera into a single frame, transferring it to the Host Computer. The Host Computer implements defect detection and classification algorithms and it takes the discard decisions, communicating them to a Cutting and Discarding Machine [4]. Discard decisions are taken considering parameters glass production process, some of which are settled via a usable operator GUI [5].

The evolution of the glass production process requires both high accuracy in defects detection and faster production lines. The detection and classification of defects imposes temporal constraints on the system. The inspection system, in fact, works in pipeline, and the Image Acquisition Subsystem feeds the pipeline at a rate which is determined by the sampling rate of the line scan camera divided by the number of lines in a frame. The Defect Detection and Classification module must work with the same rate, to avoid frame loss, i.e., the sampling rate of the line scan camera enforces an upper bound to the processing time of defect detection and classification algorithms. The current requirement of increasing the production speed involves the use of line scan cameras with increased sampling rate to keep constant or to improve the accuracy of defects detection. Consequently, the increase of production speed determines the need to reduce the processing time of defect detection and classification algorithms.

To reduce the processing time, we propose an algorithm that reduces the size of the images to be investigated by excluding subareas that can be assumed to not include defects.

As an example, we consider the critical production of glass tubes,

converted into pharmaceutical containers such as vials, syringes, and carpules.

Due to imperfections in the raw materials used in the furnace, this type of glass may have defects such as knot inclusions (blobs) or flexible fragments called lamellae, which can cause subsequent problems and pharmaceutical recalls [6], [7], [8]

The main classes of defects relevant for pharmaceutical glass production [1], [9] due to critical size features and their significant effects on the final quality of the tubes are:

- 1) air lines due to the presence of air bubbles in the furnace which are pulled by the drawing machine; they appear as darker lines of long dimensions with a back illuminator, with the end parts thinner than the center one. This line, when it is too close to the tube surface, breaks and therefore is thinner and more difficult to detect.
- 2) knot inclusion (blobs) due to imperfections in the raw materials used in the furnace; they appear on the tube surface as circular lenses, while they appear on the captured image as dark patches, orthogonal to the frame.

Results on a set of test images show that the proposed solution does not compromise the quality of the detection and allows to achieve an improvement of a factor of 7x compared to the existing solutions under particular conditions, with the same accuracy in defect detection.

The paper is organized as follow: in Section 2, we present the state of the art related to the system, and in Section 3 we present the rational of the proposal. In Section 4, we explain the proposed algorithm and we report the experimental results in Section 5. Conclusion are given in Section 6.

2. STATE OF THE ART

As usually done in inspection systems, the kinds of elaborations performed on each frame can mainly be divided into 3 stages [2], [10], [11].

1. Image preprocessing
2. Defects detection
3. Defects classification

In the pre-processing phase, algorithms are used to prepare the image for the following stages, with the aim of reducing detection errors due to the acquisition process. The steps generally adopted concern noise reduction, contrast enhancement [12], elimination of unwanted regions and identification of the region of interest (ROI).

In glass tube production, state-of-the-art ROI extraction techniques consist in identifying the useful part of the image inside the frame (called hereinafter Internal of the tube), excluding the dark area due to the glass surface on which the light rays of the illuminator have a critical angle of incidence

according to Snell's law. In this case, the light rays are reflected on the glass tube and do not affect the camera sensor. An algorithm to extract the internal part of the tube has been proposed in [1].

In the defect detection stage, algorithms are used to determine image regions whose pixels may identify a defect. To extract these regions, segmentation techniques are adopted [10], typically based on thresholds [3] or on edge detection [13], [14].

The classification stage consists of algorithms that extract a series of characteristics of the segmented regions, eventually including them within predetermined classes of defects.

State of the art techniques for feature/defect detection and extraction are the edge detection techniques [13]. Edge detection aims to identify points in a digital image where the image brightness changes sharply compared to the rest. Among the various edge detection techniques, the algorithm proposed by Canny [14] (Canny algorithm) is considered the ideal one for images with noise [13]. The image is first smoothed with a Gaussian filter and then gradient magnitude is computed at each pixel of the smoothed image; edges are determined by applying non-maximum suppression, double threshold, and hysteresis. The algorithm has been usefully adopted in various applications domains (inspection of semiconductor wafer surface [15], detection of defects in satin glass [16], measuring icing shape on conductor [17], studies on bubble formation in co-fed gas-liquid flows [18]) and it has been also adopted for the detection of defects in similar inspection systems [1]

Other techniques for defect detection and extraction are based on thresholds, that can be global (fixed for the whole image) or local, i.e. they can be variable in different regions of the image [19].

As for global thresholds techniques, [12] presents an inspection method for float glass fabrication. The authors utilize a benchmark image to remove bright and dull stripes that are present in their glasses. Then, they utilize adaptive global thresholds based on the OTSU algorithm [20] to separate distortions from defects. The OTSU algorithm selects threshold values (one for each image) that maximize the inter-class variance of the image histogram [21]. It is useful for separating background from defects/foreground and produces satisfactory results when images present bimodal or multimodal histograms [10]. It has been successfully utilized in [10] to derive a configurable industrial vision system for surface inspection of transparent parts (in particular, it has been tested on headlamp lens) and again in [22] to detach defects from the background in a float glass defect classificatory and in [23] or glass inspection vision systems.

By considering the characteristics of the tube glass production, the use of single or multiple constant thresholds does not allow the detection of defects. Besides, techniques based on background subtraction or other template matching techniques [3],[24] cannot be utilized due to the tube vibration and the not perfect circular section of the tube (the "sausage" shape).

As for local thresholds techniques, the Niblack's [19] binarization method is a local adaptive thresholding technique, based on varying threshold over the image by using local mean value and the standard deviation of gray level evaluated in a window centered in each pixel. This method can separate the object or text from the background effectively in the areas near to the object. Niblack method is one of the document

segmentation methods and has shown good results in segmenting text from the background. Anyway, it can be applied also to images without text [25] and has been applied in a vision system for auto seeding and for observing the surface of the melt in the Ky method for the Sapphire Crystal Growth Process [26]. In the Niblack's approach, noise still occurs in a varying manner in the background; different improvements over the original paper have been proposed, which work to improve detection or reduce the processing time [19] that makes it not suitable for real-time execution. Examples are the approach presented in [27], that proposes new thresholds to limit noise, and in [28] that applies a global threshold to each sub-image and not to each single pixel to reduce processing time.

3. THE ROI EXTRACTION

All techniques extract a ROI from the acquired image by removing the part of the image (Fig. 1) that is not belonging to the inspection object ([1], [16]). Only in [23] is presented a technique that identifies not defective areas within the ROI (background) using a threshold on the local variance calculated in a window centered on each pixel (values of the variance lower than a threshold identify regions without defect). In that paper, statistics on areas without error are used to automatically calculate the thresholds to perform segmentation, more accurately than OTSU.

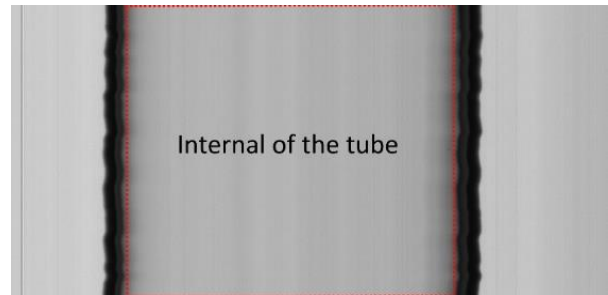


Fig. 1. Image taken by the line-scan camera. The array of CCD sensors in the line scan camera is orthogonal to the direction of the movement of the tube (tube direction). The internal of the tube is also highlighted. It represents the portion of the image which is further analyzed for detecting the column with defect for segmentation. The frame is composed of 1000x2048 pixels.

Our idea is to remove areas where it is possible to easily predict that no defects are present (reducing the size of the ROI). State of the art defect detection techniques examine the entire internal area of the tube. They waste processing time if it is known that some of these parts do not contain defects.

We observe that, since the luminous intensity inside a column is almost constant except in pixels where there is noise or defects, the standard deviation of each column can be used as an indicator of the presence of a defect on that column. Therefore, values of the standard deviation of a column below a certain threshold indicate that the column can be excluded by the following elaborations. Anyway, the standard deviation of the columns is also influenced by the alignment of the illuminator with the acquisition camera. In case of not perfect alignment, the standard deviation shows an increasing trend from one edge of the tube to the other, which can be approximated with a linear trend. In order to avoid any influence from this factor, we consider the values of the standard deviation of the columns removing their linear trend (Detrended Standard Deviation - DSD).

Another relevant requirement concerns the ability to accurately detect the size of defects. We have experimented that luminous

intensity of the defects presents high values near the central area of the defects but tends to decrease away from it. Therefore, not all the columns including a defect have high standard deviation value. Applying a single threshold on the DSD can then lead to an inaccurate detection of the size of the defects. Anyway, a defect includes columns with DSD over a certain threshold, and columns adjacent to those with lower DSD values. To detect these columns, we apply two hysteresis thresholds (t_L and t_H with $t_L < t_H$) algorithm. Columns with DSD values less than t_L are not considered to belong to ROI, columns with values greater than t_H are considered to belong to ROI and column with values between t_L and t_H are considered to belong to ROI only if they are adjacent to columns that belong to ROI.

Using DSD criterion, areas near the edge of the tube are often classified as ROI, as they have peaks of DSD greater than the peaks of the DSD of the columns where defects are placed. These values are caused by many effects as the vibration of the moving tube or the imperfect circular shape of the tube. In these areas, there may be defects. A solution is to exclude the ROIs located near the edges. This solution is not destructive because, in the case of glass tube, 3 cameras and illuminators are utilized to have a 360 degrees inspection, and areas near the edges for a camera appear in central area for one of the other two (positioned at 120 degrees from it and the tube). So, the solution to exclude areas near the edge of the tube seems the most appropriate to reduce again the time execution.

4. ALGORITHM

The proposed algorithm (Detrended Standard Deviation ROI Reduction algorithm, DSDRR), starting from the image calculates for each column the DSD. Then, the algorithm finds the columns whose DSD values are greater than a t_H threshold and promotes all these columns as belonging to the ROI. Next, for each of the columns belonging to the ROI, the algorithm finds the adjacent columns whose DSD values are greater than t_L and promotes also these columns as belonging to the ROI. If ROI of areas close to the edge of the tube must be excluded from the analysis, the algorithm removes from the ROIs the columns adjacent to the first and the last column.

The choice of the threshold values used in the algorithm determines algorithm performance. It can cause the exclusion of defects in the ROIs (causing false negative in detection), or it can generate too large ROI with no reduction of the overall processing time.

The choice of threshold t_H must guarantee that at least one column of a defect belongs to the ROI, i.e. the DSD for that columns is higher than t_H . To ensure that all the defects are correctly included in the ROI, the threshold t_H must be chosen lower than the maximum values of the DSD of the columns of all the defects. As t_H threshold increases, the number of zones included in the ROI decreases. Too high values of t_H can exclude from the ROI areas that include defects. As t_H threshold decreases, the number of zones included in the ROI increases. Too low values of t_H , therefore, lead to extremely large ROI. The choice of threshold t_L must guarantee that all the columns of a defect belong to the ROI, otherwise a portion of the defect are not detected, thus limiting the quality of detection. Too high value of t_L could exclude portions of the shape of the defect from the ROI. Too low values of t_L could cause again the ROI to include the entire internal of the tube. A possible solution is to set it to a value lower than the minimum value of the DSD of the

columns of all the defects. This ensures that, if a defect is detected using threshold t_H , its entire shape is included in the ROI.

5. RESULTS

The inspection system has been implemented and it is working on production lines of a glass tube foundry [1]. The algorithm has been implemented in OpenCV [29], [30] and the image processing pipeline runs as a task activated by the frame grabber when a new frame is ready in main memory. Table I summarizes the main features of the Host Computer, the algorithms utilized for the various stages of defect detection and their configuration parameters. All the image processing algorithms have been implemented using the OpenCV library [29], [30] and compiled with the Visual Studio compiler.

Hardware Configuration			
Processor	Intel® Core™ i7-940 Processor (8MB Cache, 2.93 GHz)		
RAM	8 GB		
Defect detection system			
Algorithm name	Without DSDRR	DSDRR with edges	DSDRR no edges
ROI extraction	Internal part	Internal part + DSDRR including edges with $t_L=0$, $t_H=2$	Internal part + DSDRR excluding edges with $t_L=0$, $t_H=2$
Defect Detection	Canny (35,80) or MAGDDA (ws = 145, k=10.7)		
Implementation	OPENCV		

This section shows the application of the algorithm on a set of images acquired during the production phase. All frames are composed of 1000 lines acquired by the line scan camera sensor (2K pixels). These frames contain defects with critical shape or position characteristics that make it difficult to detect, classify or include them in an ROI with the proposed algorithm. The machine on which tests are executed has a configuration like the production one and is equipped with an Intel Core i7-940 CPU running at 2.93 GHz. As for processing time, we perform 1000 executions for each frame [31], we take for each frame the maximum total processing time.

Our proposal may be applied to any defect detection algorithm. In our experiment, we utilized two algorithms that have been successfully applied in the inspection of pharmaceutical glass tube: the Canny algorithm [14] and the MAGDDA [32]. With Canny, the image is first smoothed with a Gaussian filter and then gradient magnitude is computed at each pixel; edges (marked pixels) are determined via non-maximum suppression, double threshold, and hysteresis. MAGDDA algorithm [32] works at row level and apply to the ROI a moving average filter of an assigned window. Then applies a fixed threshold (k), to mark the pixel.

As for the Defect Classification stage, we adopt an algorithm that groups adjacent marked pixels using connected-components labeling and builds, for each group, the smallest rectangle that contains them. Measurements on the rectangle permits to individuate blobs and air lines. In the tested image-set, DSDRR is applied using thresholds $t_H = 2$ and $t_L = 0$. For each frame are reported: i) the ROI calculated with traditional approach (described in [1]), ii) the graph of the DSD values calculated on the columns and thresholds $t_H = 2$ and $t_L = 0$ and iii) the ROI calculated by the application of the DSDRR algorithm on these frames with $t_H = 2$ and $t_L = 0$.

Cases of air line defects

Fig. 2 contains a frame with an air line defect. DSD values are high in the central part of the defect but rotation and vibration cause DSD values not particularly elevated on the columns of the tails of the air line. The double threshold with hysteresis however succeeds in capturing the entire shape of the defect which is

completely included in the ROI. Fig. 3 shows a frame with an air line defect. In this case, the effects of rotation and vibration are not particularly prominent. The defect then appears as a straight and dark line and this causes particularly high DSD values. The proposed thresholds are therefore useful to capture and include this defect in the ROI. However, this defect spans two distinct frames. Fig. 4 contains a frame with the tail of the air line of Fig 3. The entire shape of the defect spans two different frames. The reported frame contains a smaller fraction of the entire shape of the defect and therefore the value of the DSD experiences a smaller variation than it would have if all the defect were included in the frame. Despite this situation, the thresholds presented are sufficient to locate the defect and allow the DSDRR algorithm to include it in the ROI. Fig. 5 shows a frame with two air line on the two faces of the tube. These defects have different lengths and have shape variations due to rotation and vibration. In particular, the shorter defect has a lighter luminous intensity than the other defect, and therefore the DSD values are lower. In this case, only a few columns have a DSD value greater than the t_H threshold, so this defect is included in the ROI. Since all defect columns have a DSD value greater than t_L , then the entire defect shape is included in the ROI. The analysis of this frame underlines that lower values of the t_H threshold can exclude from the ROI the defect and therefore cause a false negative in the phase detection.

Cases of blob defects

Fig. 6 shows a frame with a blob defect. This defect, although small, has very low luminous intensity values, so the DSD values on the columns are very high compared to those on the defect-free columns. On the right side of the image, it is possible to see lightning effects that are not perfectly aligned. Removing the trend from the standard deviation values allows these defect-free areas to be removed from the ROI.

In Fig. 7 the blob defect is located in a ROI near the edge of the tube. The exclusion of this area from the ROI algorithm leads to a false negative in the inspection of this frame. However, this blob is centrally located in the frame acquired from another camera, so to reduce processing time areas near the edges of the tube can be removed. Fig. 8 shows a frame with 3 blob defects. The presence of multiple defects located in the same columns bring an increase in DSD values, therefore their inclusion in the ROI becomes particularly efficacious.

Case of frame without defects

Fig. 9 shows a frame without defects. On the right side of the frame are visible effects due to the wavy shape of the tube and the presence of dust on the surface of the glass. These effects cause high DSD values leading to the inclusion of these areas in the ROI. The classification subsystem can correctly detect the absence of defects in this frame. DSDRR returns an empty ROI on frames without defects and without effects due to noise.

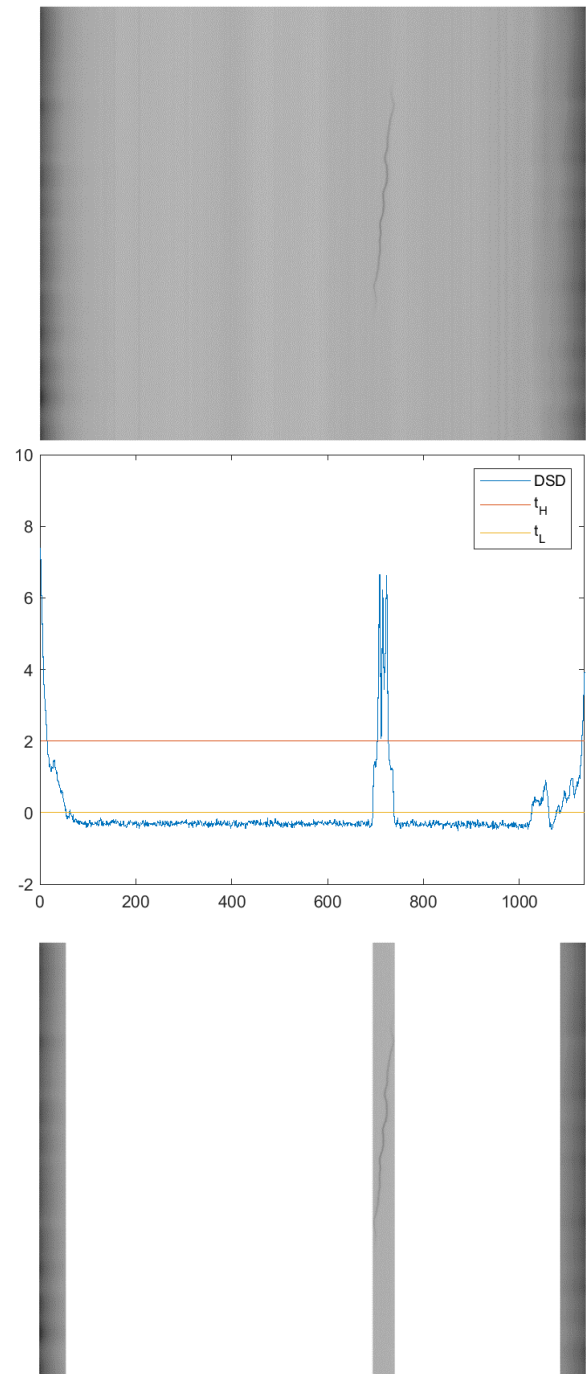


Fig. 2 i) the ROI calculated with traditional approach ii) the graph of the DSD values calculated on the columns of the extracted ROI and the proposed thresholds iii) the reduced ROI applying DSDRR algorithm with proposed thresholds ($t_H = 2$ and $t_L = 0$).

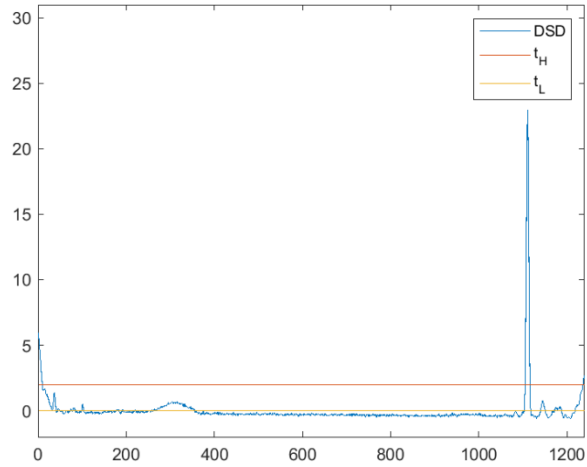
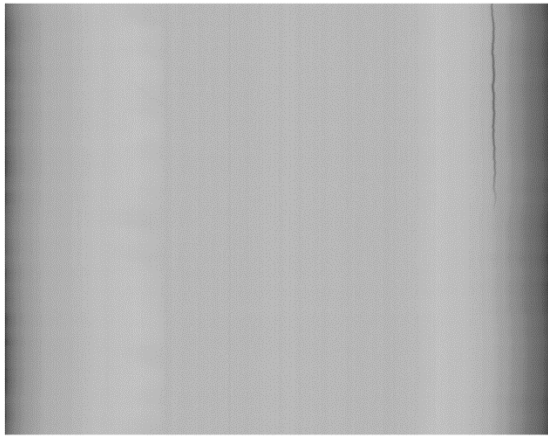


Fig. 3 i) the ROI calculated with traditional approach ii) the graph of the DSD values calculated on the columns of the extracted ROI and the proposed thresholds iii) the reduced ROI applying DSDRR algorithm with proposed thresholds ($t_H = 2$ and $t_L = 0$).

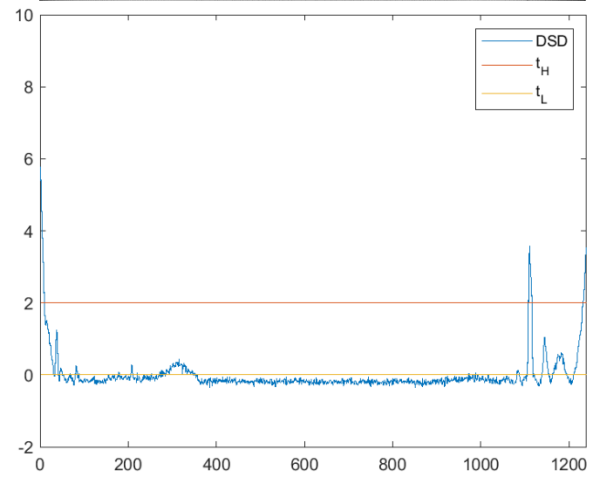
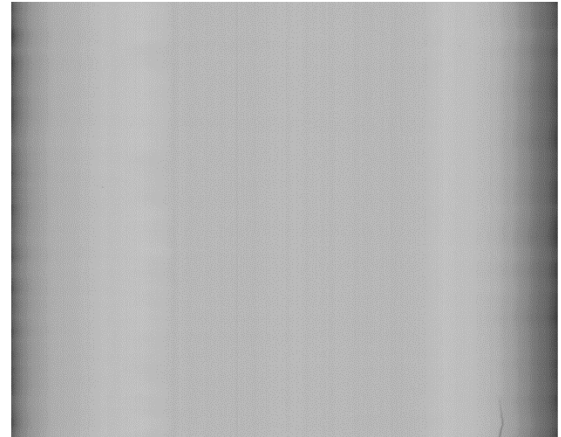


Fig. 4 i) the ROI calculated with traditional approach ii) the graph of the DSD values calculated on the columns of the extracted ROI and the proposed thresholds iii) the reduced ROI applying DSDRR algorithm with proposed thresholds ($t_H = 2$ and $t_L = 0$).

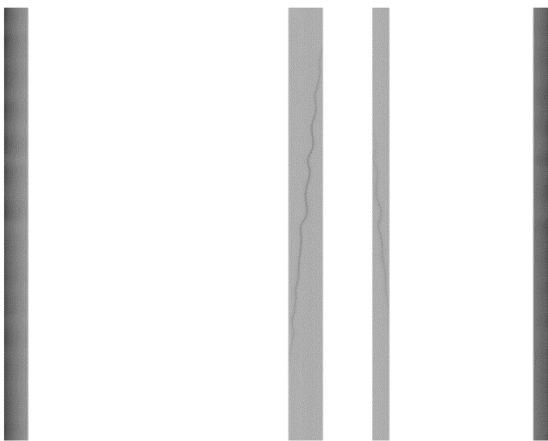
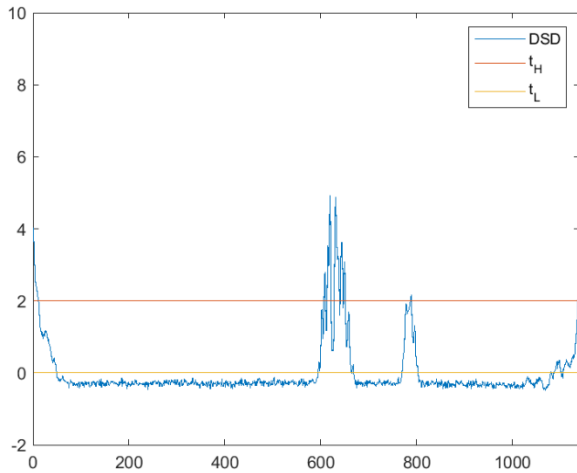
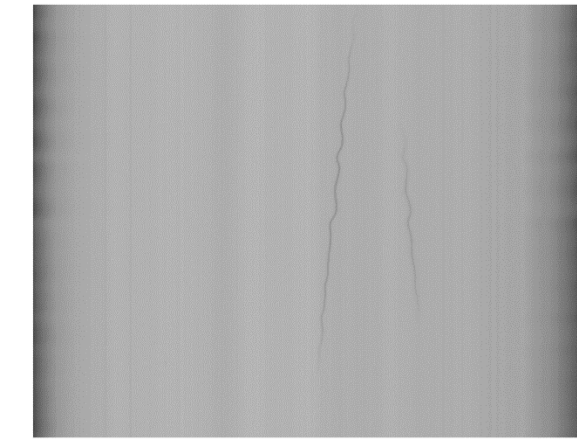


Fig. 5 i) the ROI calculated with traditional approach ii) the graph of the DSD values calculated on the columns of the extracted ROI and the proposed thresholds iii) the reduced ROI applying DSDRR algorithm with proposed thresholds ($t_H = 2$ and $t_L = 0$).

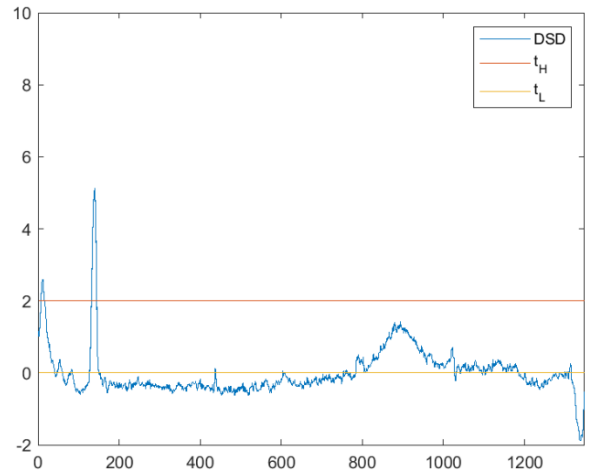


Fig. 6 i) the ROI calculated with traditional approach ii) the graph of the DSD values calculated on the columns of the extracted ROI and the proposed thresholds iii) the reduced ROI applying DSDRR algorithm with proposed thresholds ($t_H = 2$ and $t_L = 0$).

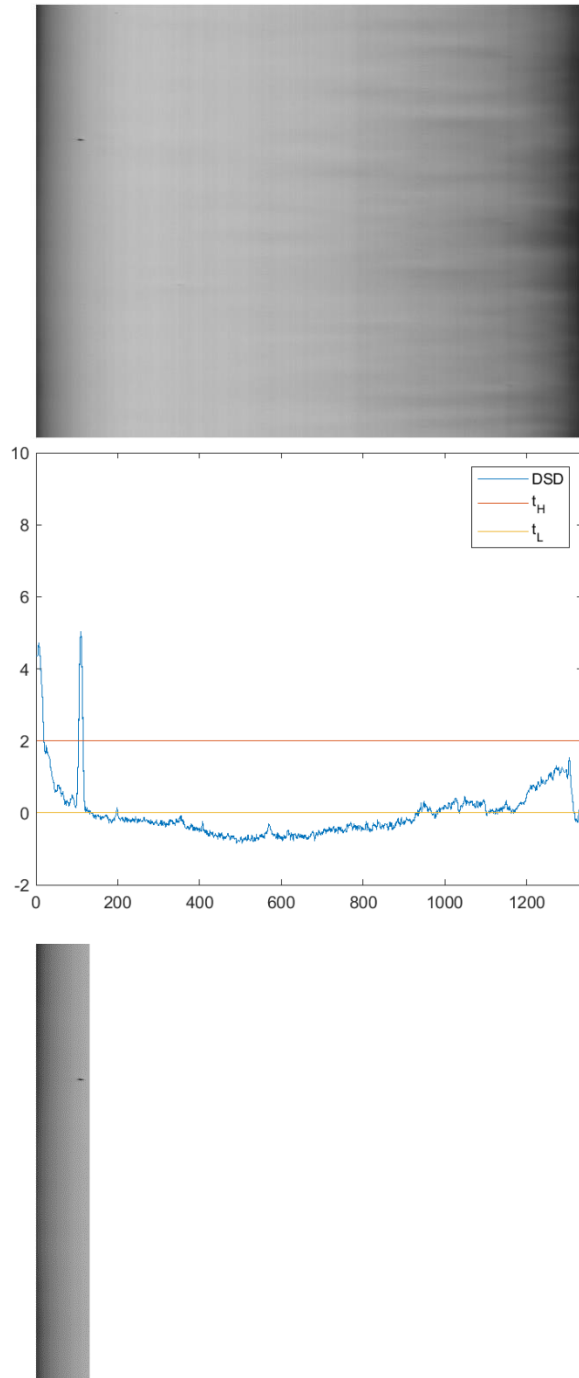


Fig. 7 i) the ROI calculated with traditional approach ii) the graph of the DSD values calculated on the columns of the extracted ROI and the proposed thresholds iii) the reduced ROI applying DSDRR algorithm with proposed thresholds ($t_H = 2$ and $t_L = 0$).

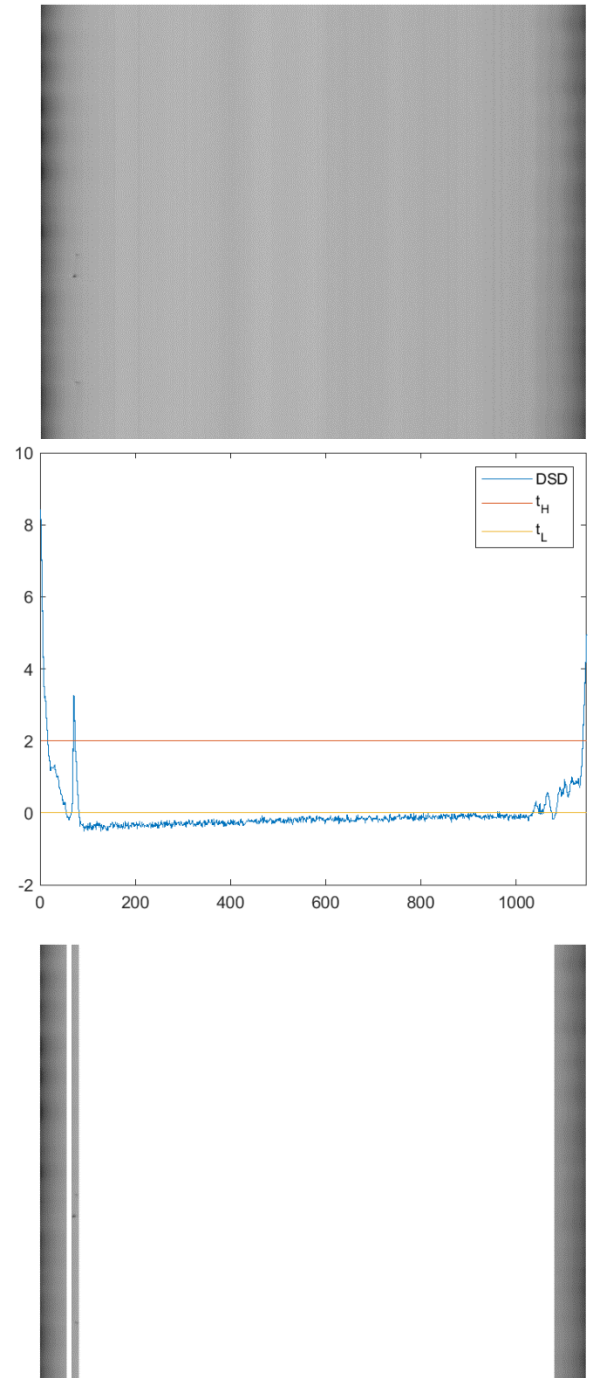
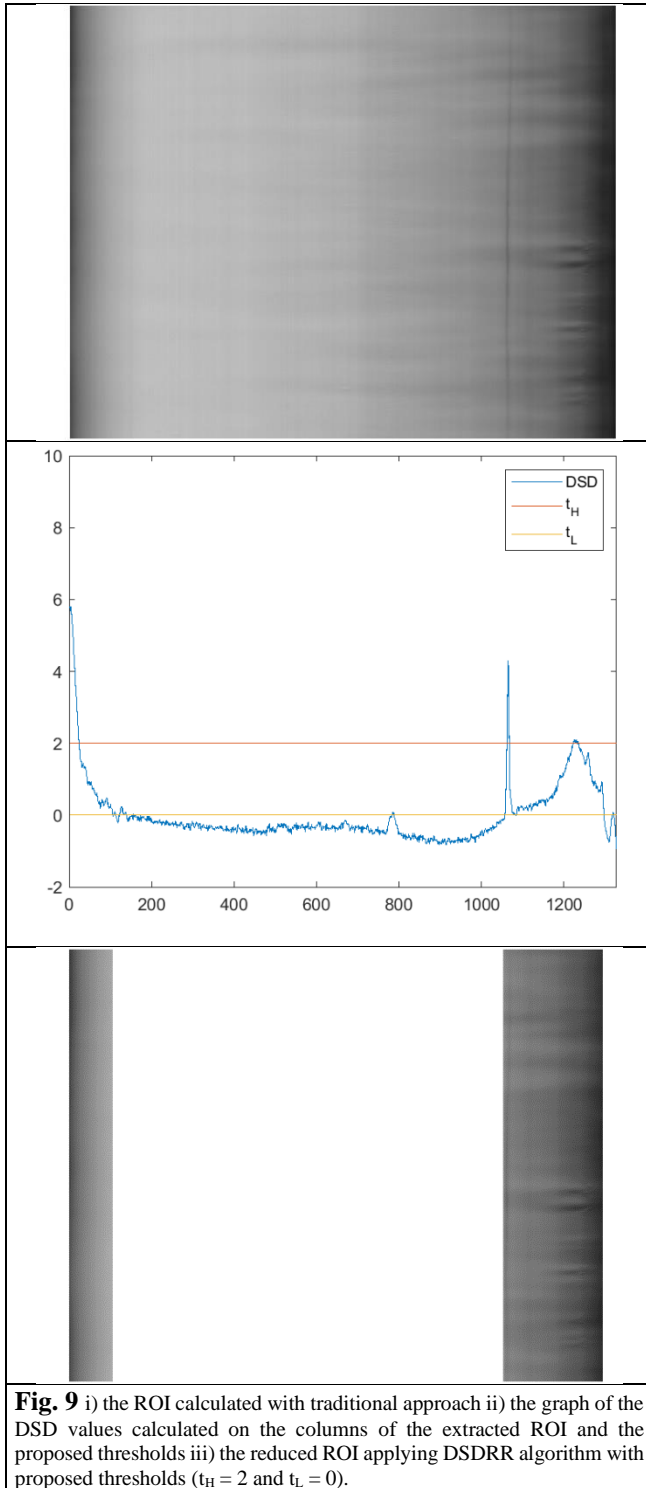


Fig. 8 i) the ROI calculated with traditional approach ii) the graph of the DSD values calculated on the columns of the extracted ROI and the proposed thresholds iii) the reduced ROI applying DSDRR algorithm with proposed thresholds ($t_H = 2$ and $t_L = 0$).



Processing Times

For each of the proposed frames, Table II shows the parameters measured during their processing. In detail, we have reported:

- the measurement of the ROI examined (as number of columns)
- the maximum processing time of the entire frame using the Canny algorithm
- the maximum processing time of the entire frame using the MAGDDA algorithm using the traditional and DSDRR approach as for ROI calculation, including and excluding areas close to the pipe edges.

TABLE II PROCESSING TIMES OF THE EXAMINATED FRAMES			
	Without DSDRR	DSDRR with edge	DSDRR without edge
Frame of Fig 2			
ROI (# of columns)	1136	154	46
CANNY	86.253 ms	37.145 ms	29.698 ms
MAGDDA	30.875 ms	18.112 ms	15.541 ms
Frame of Fig 3			
ROI (# of columns)	1240	81	16
CANNY	77.587 ms	33.258 ms	24.980 ms
MAGDDA	23.185 ms	16.090 ms	14.222 ms
Frame of Fig 4			
ROI (# of columns)	1240	79	16
CANNY	76.968 ms	33.202 ms	24.771 ms
MAGDDA	23.001 ms	15.814 ms	14.081 ms
Frame of Fig 5			
ROI (# of columns)	1140	194	108
CANNY	86.843 ms	36.092 ms	29.687 ms
MAGDDA	32.198 ms	19.025 ms	16.118 ms
Frame of Fig 6			
ROI (# of columns)	1348	66	24
CANNY	82.583 ms	33.286 ms	24.968 ms
MAGDDA	27.693 ms	17.286 ms	15.108 ms
Frame of Fig 7			
ROI (# of columns)	1336	131	0
CANNY	79.289 ms	34.985 ms	11.397 ms
MAGDDA	23.925 ms	17.898 ms	11.358 ms
Frame of Fig 8			
ROI (# of columns)	1148	138	16
CANNY	75.286 ms	32.869 ms	19.682 ms
MAGDDA	22.524 ms	14.625 ms	13.893 ms
Frame of Fig 9			
ROI (# of columns)	1328	348	242
CANNY	89.677 ms	37.281 ms	23.714 ms
MAGDDA	23.926 ms	19.628 ms	17.002 ms

As regards the measurement of ROI, compared to the area of the internal parts of the tube, the ROI is reduced on average by 88%, and at most by 95% and at least by 74%. Excluding the parts near the edges of the tube, the ROI is reduced on average by 95% and at most by 100% (in frames without defects) and at least by 82%. The reduced area of the ROI has a direct impact on the processing time of the further stages of detection, and in the overall processing time. The processing times of entire process using Canny have an increase in performance of a factor 2.5x in the best case using DSDRR including edges of the tube and of a factor 7x excluding edges. For MAGDDA, the factors are 1.7x including edges and 2.1x excluding edges of the tube.

In particular, in cases where the frames do not contain defects, the proposed algorithm does not detect ROIs and the execution of subsequent stages of detection and classification and reducing waste of processing time.

Since the processing period must be lower than the acquisition period, a reduction of the processing time allows the use of cameras with a higher sample rate or to increase the speed of production without loss of accuracy in defects recognition.

6. CONCLUSION

A vision system can be exploited to inspect the quality of glass products during the production process. Improvements in such processes and the need to increase the accuracy of detection suggest the adoption of solutions that reduce the processing time of all the steps involved in defect detection and classification. A classical approach for dealing with inspection consists in extracting the whole internal part of the product (ROI) and pass it to defect detection and classification algorithm. In this paper, we proposed and analyzed the idea of further reducing the ROI area by excluding columns that can be assumed to not include defects, with a consequent reduction in the processing time. As a proof of concept, we apply the idea to the inspection of pharmaceutical glass tubes. Detrended Standard Deviation can be exploited to compensate the effects of not perfect alignment of camera and illuminator, and we utilize a double threshold with hysteresis algorithm to detect column belonging to the ROI that must be investigated. Results of a set of typical image show that our proposal does not change the quality of detection of the system and significantly improves processing time of both defect detection and classification stages. Processing time can be reduced of a factor 7x in frames without defects. The idea of reducing the ROI is general: as for future works, we plan to quantify its effectiveness in other application domains, and to investigate strategies to parallelize the algorithms by considering advanced CMPs and the GPU architectures and their memory hierarchy [33].

7. ACKNOWLEDGMENTS

This work has been partially supported by the Italian Ministry of Education and Research (MIUR) in the framework of the CrossLab project (Departments of Excellence – LAB Advanced Manufacturing and LAB Cloud Computing, Big data & Cybersecurity)

8. REFERENCES

- [1] P. Foglia, C.A. Prete, M. Zanda, An inspection system for pharmaceutical glass tubes, WSEAS Transactions on Systems, Vol. 14, Art. #12, PP. 123-136, 2015
- [2] Kumar, Ajay. "Computer-vision-based fabric defect detection: A survey." *IEEE trans. on ind, electronics* 55.1 (2008): 348-363.
- [3] Peng, Xiangqian, et al. An online defects inspection method for float glass fabrication based on machine vision. *The International Journal of Advanced Manufacturing Technology* 39.11-12 (2008): 1180-1189.
- [4] S. Campanelli, P. Foglia, C.A. Prete. An architecture to integrate IEC 61131-3 systems in an IEC 61499 distributed solution, *Computers in Industry*, Vol. 72, Sept. 2015, pp. 47-67.
- [5] P. Foglia, et al. Towards relating physiological signals to usability metrics: A case study with a web avatar (2014) WSEAS Transactions on Computers, 13, pp. 624-634.
- [6] Reynolds G, Peskiet D. Glass delamination and breakage, new answers for a growing problem; *BioProcess International* 9(11):52-57, 2011.
- [7] Iacocca R.G., Toldt N., et al.. Factors Affecting the Chemical Durability of Glass Used in the Pharmaceutical Industry. *AAPS PharmSciTech*, v.11(3):1340-1349, 2010.
- [8] Schaut, Robert A., and W. Porter Weeks. "Historical review of glasses used for parenteral packaging." *PDA journal of pharmaceutical science and technology*, 71.4 (2017): 279-296.
- [9] Berry H. *Pharmaceutical aspects of glass and rubber*; J. of Pharmacy and Pharmacology, v.5(11):1008-1023; Wiley, 2011.
- [10] Martínez, S. Satorres, et al. "An industrial vision system for surface quality inspection of transparent parts." *The International Journal of Advanced Manufacturing Technology* 68.5-8 (2013): 1123-1136

- [11] Malamas, N., et al. "A survey on industrial vision systems, applications and tools." *Image and vision computing* 21.2 (2003): 171-188.
- [12] Li, Di, Lie-Quan Liang, and Wu-Jie Zhang. "Defect inspection and extraction of the mobile phone cover glass based on the principal components analysis." *The International Journal of Advanced Manufacturing Technology* 73.9-12 (2014): 1605-1614.
- [13] Kumar, Mukesh, Rohini Saxena. "Algorithm and technique on various edge detection: A survey." *Signal & Image Processing* 4.3 (2013): 65.
- [14] J.F. Canny, A computational approach to edge detection, *IEEE Trans. Pattern Analysis and Machine Intelligence*, 8(6):679-698, 1986
- [15] N.G. Shankar, Z.W. Zhong, Defect detection on semiconductor wafer surfaces, *Microelectronic Engineering*, 77 (3-4), 337-346, 2005
- [16] Adamo, Francesco, et al. "A low-cost inspection system for online defects assessment in satin glass." *Measurement* 42.9 (2009): 1304-1311.
- [17] Xinbo Huang, et al, An Online Technology for Measuring Icing Shape on Conductor Based on Vision and Force Sensors, *IEEE Transactions on Instrumentation and Measurement*, 66 (12) 3180-3189, 2017.
- [18] M.M. de Beer, et al., Bubble formation in co-fed gas-liquid flows in a rotor-stator spinning disc reactor, *International Journal of Multiphase Flow*, Volume 83, 2016, pp 142-152.
- [19] Saxena, Lalit Prakash. "Niblack's binarization method and its modifications to real-time applications: a review." *Artificial Intelligence Review* (2017): 1-33.
- [20] Otsu N, A threshold selection using an iterative selection method. *IEEE Trans Syst Man Cybern* (1979) 9:62-66
- [21] Zouhir Wakaf, Hamid A. Jalab, Defect detection based on extreme edge of defective region histogram, *Journal of King Saud University - Computer and Information Sciences*, Volume 30, Issue 1, 2018, Pages 33-40
- [22] L. Huai-guang et al., A classification method of glass defect based on multiresolution and information fusion, *The International Journal of Advanced Manufacturing Technology*, Vol. 56 (9), pp. 1079-1090, 2011.
- [23] Masoumeh Aminzadeh, Thomas Kurfess, Automatic thresholding for defect detection by background histogram mode extents, *Journal of Manufacturing Systems*, Vol. 37(1), pp. 83-92, 2015.
- [24] H. Kong, et al., "Accurate and Efficient Inspection of Speckle and Scratch Defects on Surfaces of Planar Products," *IEEE Trans. on Industrial Informatics*, vol. 13(4), pp. 1855-1865, Aug. 2017.
- [25] Farid, S., and F. Ahmed. "Application of Niblack's method on images." *Inter. Conf. on Emerging Technologies. IEEE*, 2009.
- [26] Kim, Churl Min, Sung Ryul Kim, and Jung Hwan Ahn. "Development of Auto-Seeding System Using Image Processing Technology in the Sapphire Crystal Growth Process via the Kyropoulos Method." *Applied Sciences* 7.4 (2017): 371.
- [27] J. Sauvola, M. Pietikäinen, Adaptive document image binarization, *Pattern Recognition*, Vol. 33(2), 2000, pp 225-236.
- [28] Kulyukin V, Kutiyawala A, Zaman T (2012) Eyes-free barcode detection on smartphones with Niblack's binarization and support vector machines. *Proc Int Conf Image Process Comput Vis Pattern Recognit* 1:284-290
- [29] Bradski, Gary, and Adrian Kaehler. *Learning OpenCV: Computer vision with the OpenCV library*. O'Reilly Media, Inc., 2008.
- [30] <https://opencv.org/>
- [31] J. Abella, M. Padilla, et al., Measurement-Based Worst-Case Execution Time Estimation Using the Coefficient of Variation, *ACM Trans. Des. Autom. Electron. Syst.* 22, 4, Article 72 (June 2017).
- [32] G.A. De Vitis, P. Foglia, C.A. Prete, "A Special Purpose Algorithm to Inspect Glass Tubes in the Production Phase", TR-DII-2018-01, University of Pisa, 2018
- [33] Bartolini, S., Foglia, P., & Prete, C. A. (2018). Exploring the relationship between architectures and management policies in the design of NUCA-based chip multicore systems. *Future Generation Computer Systems*, 78, 481-501.